DNA synthesis is detectable by fluorescence-activated cell sorting (FACS) (Fig. 5a), whereas the initiation of ori609 started at 30 min and continued until 60 min after the release to the S phase. In *rad53-1* mutant cells the early origin fired at the same time as in the wild type, whereas the late origin fired more than 10 min earlier than in the wild-type cells and continued for 30 min. In addition, the characteristic long time span of passive replication of the ori609 region in wild-type cells disappeared completely in the *rad53-1* mutant cells. Thus the timing of firing of the late origin and the regulation of replication-fork movement at the terminal region of the right half of the chromosome VI (ref. 1) are disturbed by *rad53-1* mutation. The *orc2-1* mutation affected the timing of firing of both early and late origins without affecting fork movement in the late-origin region.

Mutations in other genes involved in initiation and elongation of DNA replication (*cdc6-1*, *mcm3-1*, *pol2-11*, *dpb11-1*, *cdc47-1* and *dna2* mutants) had no effect on the block of S-phase progression although these mutants exhibited increased sensitivity to MMS. We were surprised to find that Rad53 and Orc2 are involved in regulating the efficiency of initiation of origins in normal growth conditions. In fact, a very inefficient origin on chromosome VI, ori608, was activated quite efficiently in both *rad53-1* and *orc2-1* mutants (Fig. 4a). Moreover, the timing of initiation of the late origin ori609 was markedly accelerated in the *rad53-1* mutant, and ori609 became an earlier-initiating origin (Fig. 5b). These results indicate that *rad53* is involved in determining the efficiency and timing of late-replicating origins of chromosomes by suppressing the activation of these origins. *orc2* may be involved in the regulation of activation of early origins and in suppression of late-origin firing. In both cases, the suppression of late origins is important in the cell's surveillance of S-phase progression when cells are exposed to DNA-damaging reagents.

In mammalian cells, the reduction in S-phase progression in the presence of DNA damage may be the result of inactivation of some origins[10]. For example, in CHO cells, ionizing radiation caused the inhibition of initiation of origins at the *dihydrofolate reductase* locus rather than inhibition of elongation[10,11], indicating the same downregulation system may be conserved in yeast and higher eukaryotes. □

Methods

We used the following yeast strains: W303-1A (genotype MAT-a *ade2-1 can1-100 his3-11,15 leu2-3,112 trp1-1 ura3-1*), W303-1B (genotype MAT-α *ade2-1 can1-100 his3-11,15 leu2-3,112 trp1-1 ura3-1*, both from R. Rothstein), 7830-2-4A (genotype MAT-a *his3 leu2 ura3 trp1*), DLY264 (genotype MATa *rad53-1* (7830-2-4A background), DLY285 (genotype MATa *mec1-1 sml1* (7830-2-4A background), all three from L. H. Hartwell), JRY4125 (genotype MAT-α *orc2-1* (W303 background), from J. Rine), YHY201A (genotype MAT-a *orc2-1* (W303 background)), and YHY301A (genotype MAT-a *rad53-1* (W303 background)).

Cell-cycle arrest and two-dimensional gel-electrophoresis analyses of replication intermediates have been described[2,12]. Initiation and replication time analyses were performed as described[2]. FACS analyses were done as described[3].

Received 16 July; accepted 7 August 1998.

1. Friedman, K. L., Brewer, B. J. & Fangman, W. L. Replication profile of *Saccharomyces cerevisiae* chromosome VI. *Genes Cells* **2,** 667–678 (1997).
2. Yamashita, M. *et al.* The efficiency and timing of initiation of replication of multiple replicons of *Saccharomyces cerevisiae* chromosome VI. *Genes Cells* **2,** 655–665 (1997).
3. Paulovich, A. G. & Hartwell, L. H. A checkpoint regulates the rate of progression through S phase in *S. cerevisiae* in response to DNA damage. *Cell* **82,** 841–847 (1995).
4. Elledge, S. J. Cell cycle checkpoints: preventing an identity crisis. *Science* **274,** 1664–1672 (1996).
5. Nasmyth, K. Viewpoint: putting the cell cycle in order. *Science* **274,** 1643–1645 (1996).
6. Foss, M., McNally, F. J., Laurenson, P. & Rine, J. Origin recognition complexes (ORC) in transcriptional silencing and DNA replication in *S. cerevisiae*. *Science* **262,** 1838–1844 (1993).
7. Bell, S. P., Kobayashi, R. & Stillman, B. Yeast origin recognition complex functions in transcription silencing and DNA replication. *Science* **262,** 1844–1849 (1993).
8. Paulovich, A. G., Margulies, R. U., Garvik, B. M. & Hartwell, L. H. *RAD9*, *RAD17*, and *RAD24* are required for S phase regulation in *Saccharomyces cerevisiae* in response to DNA damage. *Genetics* **145,** 45–62 (1997).
9. Ferguson, B. M., Brewer, B. J., Reynolds, A. E. & Fangman, W. L. A yeast origin of replication is activated late in S phase. *Cell* **65,** 507–515 (1991).
10. Larner, J. M., Lee, H. & Hamlin, J. L. Radiation effects on DNA synthesis in a defined chromosomal replicon. *Mol. Cell. Biol.* **14,** 1901–1908 (1994).
11. Lee, H., Laner, J. M. & Hamlin, J. L. A p53-independent damage-sensing mechanism that functions as a checkpoint at the G1/S transition in Chinese hamster ovary cells. *Proc. Natl Acad. Sci. USA* **94,** 526–531 (1997).
12. Hori, Y., Shirahige, K., Obuse, C., Tsurimoto, T. & Yoshikawa, H. Characterization of a novel *CDC* gene (*ORC1*) partly homologous to *CDC6* of *Saccharomyces cerevisiae*. *Mol. Biol. Cell* **7,** 409–418 (1996).

Acknowledgements. We thank J. Rine and B. Stillman for the *orc2-1* mutant and its parental strain; L. H. Hartwell for the *rad53-1* mutant, the *mec1-1* mutant and their parental strain (7830-2-4A); and J. F. X. Diffley for critical reading of this manuscript and for unpublished results. This work was supported by grants-in-aid for Cooperative Research and for Special Projects Research from the Ministry of Education, Science and Culture, Japan, and by Special Coordination Funds for promoting Science and Technology from the Science and Technology Agency of the Japanese Government.

Correspondence and requests for materials should be addressed to H.Y. (e-mail: hyoshika@bs.aist-nara.ac.jp).

erratum

Optical alignment and spinning of laser-trapped microscopic particles

M. E. J. Friese, T. A. Nieminen, N. R. Heckenberg & H. Rubinsztein-Dunlop

Nature **394,** 348–350 (1998)

The three sequential frames that should have been depicted in Fig. 1 were in fact all identical. The correct sequence is shown here. □

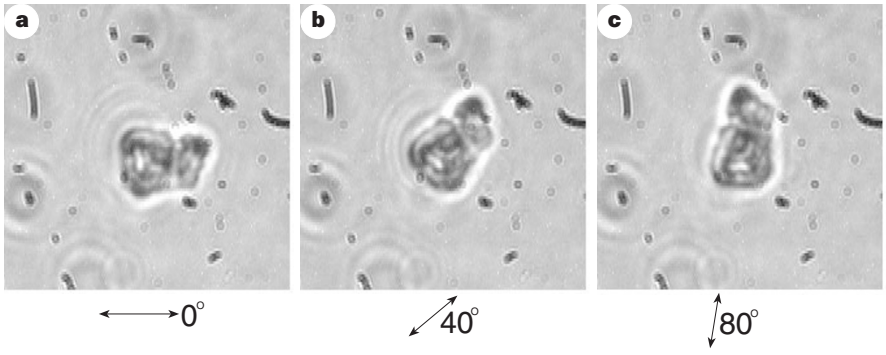

the mean orbital period derivative of $<10^{-11}$ could be reached in less than a year of observations. □

Received 29 April; accepted 16 June 1998.

1. Backer, D. C., Kulkarni, S. R., Heiles, C., Davis, M. M. & Goss, W. M. A millisecond pulsar. *Nature* **300,** 615–618 (1982).
2. Bhattacharya, D. & van den Heuvel, E. P. J. Formation and evolution of binary and millisecond pulsars. *Phys. Rep.* **203,** 1–124 (1991).
3. Wijnands, R. & van der Klis, M. A millisecond pulsar in an X-ray binary system. *Nature* **394,** 344–346 (1998).
4. Fruchter, A. S. *et al*. The eclipsing millisecond pulsar PSR 1957+20. *Astrophys. J.* **351,** 642–650 (1990).
5. Nice, D. J. & Thorsett, S. E. Pulsar PSR 1744–24A: timing, eclipses, and the evolution of neutron star binaries. *Astrophys. J.* **397,** 249–259 (1992).
6. Manchester, R. N. *et al*. Discovery of ten millisecond pulsars in the globular cluster 47 Tucanae. *Nature* **352,** 219–221 (1991).
7. Deich, W. T. S. *et al*. The binary pulsar PSR 1908+00 in NGC 6760. *Astrophys. J.* **410,** L95–L98 (1993).
8. Stappers, B. W. *et al*. Probing the eclipse region of a binary millisecond pulsar. *Astrophys. J.* **465,** L119–L122 (1996).
9. in 't Zand, J. J. *et al*. Discovery of the X-ray transient SAX J1808.4–3658, a likely low-mass X-ray binary. *Astron. Astrophys.* **331,** L25–L28 (1998).
10. Lewin, W. H. G., van Paradijs, J. & Taam, R. E. in *X-Ray Binaries* (eds Lewin, W. H. G., van Paradijs, J. & van den Heuvel, E. P. J.) 175–232 (Cambridge Univ. Press, 1995).
11. Marshall, F. E. SAX J1808.4–3658 = XTE J1808–369. *IAU Circ.* No. 6876 (1998).
12. Wijnands, R. & van der Klis, M. SAX J1808.4–3658 = XTE J1808–369. *IAU Circ.* No. 6876 (1998).
13. White, N. E., Nagase, F. & Parmar, A. N. in *X-Ray Binaries* (eds Lewin, W. H. G., van Paradijs, J. & van den Heuvel, E. P. J.) 1–57 (Cambridge Univ. Press, 1995).
14. Chakrabarty, D. & Morgan, E. H. SAX J1808.4–3658 = XTE J1808–369. *IAU Circ.* No. 6877 (1998).
15. Lyne, A. G. & Graham-Smith, F. *Pulsar Astronomy* (Cambridge Univ. Press, 1990).
16. Roche, P. *et al*. SAX J1808.4–3658 = XTE J1808–369. *IAU Circ.* No. 6885 (1998).
17. Giles, A. B., Hill, K. M. & Greenhill, J. G. SAX J1808.4–3658 = XTE J1808–369. *IAU Circ.* No. 6886 (1998).
18. Thorsett, S. E. & Chakrabarty, D. Neutron star mass measurements. I. Radio pulsars. *Astrophys. J.* (submitted); preprint astro-ph/9803260 at ⟨http://xxx.lanl.gov⟩ (1998).
19. van Kerkwijk, M. H., van Paradijs, J. & Zuiderwijk, E. J. On the masses of neutron stars. *Astron. Astrophys.* **303,** 497–501 (1995).
20. Zhang, W., Strohmayer, T. E. & Swank, J. H. Neutron star masses and radii as inferred from kilohertz quasi-periodic oscillations. *Astrophys. J.* L167–L170 (1997).
21. Faulkner, J., Flannery, B. P. & Warner, B. Ultrashort-period binaries. II. HZ 29 (=AM CVn): a double-white-dwarf semidetached postcataclysmic nova? *Astrophys. J.* **175,** L79–L83 (1972).
22. Savonije, G. J., de Kool, M. & van den Heuvel, E. P. J. The minimum orbital period for ultra-compact binaries with helium burning secondaries. *Astron. Astrophys.* **155,** 51–57 (1986).
23. Paczynski, B. Gravitational waves and the evolution of close binaries. *Acta Astron.* **17,** 287–296 (1967).
24. Tout, C. A., Pols, O. R., Eggleton, P. P. & Han, Z. Zero-age main-sequence radii and luminosities as analytic functions of mass and metallicity. *Mon. Not. R. Astron. Soc.* **281,** 257–262 (1996).
25. Podsiadlowski, P. Irradiation-driven mass transfer in low-mass X-ray binaries. *Nature* **350,** 136–138 (1991).
26. D'Antona, F. in *Evolutionary Processes in Binary Stars* (eds Wijers, R. A. M. J., Davies, M. B. & Tout, C. A.) 287–306 (Kluwer, Dordrecht, 1996).
27. Stella, L., Campana, S., Colpi, M., Mereghetti, S. & Tavani, M. Do quiescent soft X-ray transients contain millisecond radio pulsars? *Astrophys. J.* **423,** L47–L50 (1994).
28. van Paradijs, J. On the accretion instability in soft X-ray transients. *Astrophys. J.* **464,** L139–L141 (1996).
29. King, A. R., Kolb, U. & Burderi, L. Black hole binaries and X-ray transients. *Astrophys. J.* **464,** L127–L130 (1996).
30. Verbunt, F. & van den Heuvel, E. P. J. in *X-Ray Binaries* (eds Lewin, W. H. G., van Paradijs, J. & van den Heuvel, E. P. J.) 457–494 (Cambridge Univ. Press, 1995).

Acknowledgements. We thank L. Bildsten, V. Kaspi, A. Levine, R. Nelson, R. Remillard, F. Rasio, S. Thorsett, M. van der Klis and B. Vaughan for discussions, and M. Muno for assistance with the data analysis. We also thank F. Marshall, J. Swank and the RXTE team at NASA/Goddard Space Flight Center for arranging these target-of-opportunity observations and the necessary follow-up. This work was supported by NASA.

Correspondence and requests for materials should be addressed to D.C. (e-mail: deepto@space.mit.edu).

Optical alignment and spinning of laser-trapped microscopic particles

M. E. J. Friese, T. A. Nieminen, N. R. Heckenberg & H. Rubinsztein-Dunlop

Centre for Laser Science, Department of Physics, The University of Queensland, Brisbane, Queensland 4072, Australia

Light-induced rotation of absorbing microscopic particles by transfer of angular momentum from light to the material raises the possibility of optically driven micromachines. The phenomenon has been observed using elliptically polarized laser beams[1] or beams with helical phase structure[2,3]. But it is difficult to develop high power in such experiments because of overheating and unwanted axial forces, limiting the achievable rotation rates to a few hertz. This problem can in principle be overcome by using transparent particles, transferring angular momentum by a mechanism first observed by Beth in 1936[4], when he reported a tiny torque developed in a quartz 'wave-plate' owing to the change in polarization of transmitted light. Here we show that an optical torque can be induced on microscopic birefringent particles of calcite held by optical tweezers[5]. Depending on the polarization of the incident beam, the particles either become aligned with the plane of polarization (and thus can be rotated through specified angles) or spin with constant rotation frequency. Because these microscopic particles are transparent, they can be held in three-dimensional optical traps at very high power without heating, leading to rotation rates of over 350 Hz.

A typical optical-tweezers arrangement was used to trap microscopic calcite particles in three dimensions using between 30 and 300 mW of laser light at a wavelength of 1,064 nm. The optical trap used a 100× oil-immersion, high numerical aperture (NA = 1.3) microscope objective. The trapping beam was initially linearly polarized, and the plane of polarization could be rotated using a half-wave plate. Alternatively, a quarter-wave plate allowed the ellipticity of polarization to be varied. The particles were fragments obtained by crushing a small crystal, giving irregular particles 1–15 μm across. They were dispersed in distilled water in a trapping cell consisting of a well in a microscope slide with a coverslip.

Because of their birefringent nature, calcite particles can act as wave-plates; a calcite particle 3 μm thick is a λ/2 plate for 1,064-nm light. On passage through a fragment of calcite, the ordinary and extraordinary components of the incident light will undergo different phase shifts. If this results in a change in the angular momentum carried by the light, there will be a corresponding torque on the material. Our results can be understood using a simple plane-wave picture; the interaction between an incident plane wave and a wave-plate is outlined below. We note that the calcite wave-plate is trapped at the focal point of the beam, where the wavefronts are nearly plane.

An incident laser beam can in general have both circularly polarized and plane polarized components; that is, it will be elliptically polarized. Elliptically polarized light can be described by $\mathbf{E} = E_0 e^{i\omega t}\cos\phi\hat{\mathbf{x}} + iE_0 e^{i\omega t}\sin\phi\hat{\mathbf{y}}$ where ϕ describes the degree of ellipticity of the light ($\phi = 0$ or $\pi/2$ indicates plane-polarized light, $\phi = \pi/4$ circularly polarized light). The angular momentum of a plane electromagnetic wave (the incident light) of angular frequency ω can be found from the electric field $\mathbf{E}$ and its complex conjugate $\mathbf{E}^\star$ by integrating over all spatial elements d^3r giving $\mathbf{J} = (\epsilon/(2i\omega))\int d^3r\mathbf{E}^* \times \mathbf{E}$, where ϵ is the permittivity.

To calculate the change in angular momentum of the light after passage through a birefringent material, the incident elliptically polarized light is first expressed in terms of components parallel and perpendicular to the optic axis of the material by:

$$\mathbf{E} = E_0 e^{i\omega t}(\cos\phi\cos\theta - i\sin\phi\sin\theta)\hat{\mathbf{i}} + E_0 e^{i\omega t}(\cos\phi\sin\theta + i\sin\phi\cos\theta)\hat{\mathbf{j}} \quad (1)$$

where θ is the angle between the fast axis of the quarter-wave plate producing the elliptically polarized light and the optic axis of the birefringent material. The phase shift due to passing through a thickness d with refractive index n is kdn, where k is the free-space wavenumber, so the emergent light field will be

$$\mathbf{E} = E_0 e^{i\omega t} e^{ikdn_e}(\cos\phi\cos\theta - i\sin\phi\sin\theta)\hat{\mathbf{i}} + E_0 e^{i\omega t} e^{ikdn_o}(\cos\phi\sin\theta + i\sin\phi\cos\theta)\hat{\mathbf{j}} \quad (2)$$

where n_e and n_o are the refractive indices of the birefringent material experienced by extraordinary and ordinary rays, respectively.

The changes in the angular momentum of the light cause a reaction torque per unit area on the thickness d of material of:

$$\tau = -\frac{\epsilon}{2\omega}E_0^2 \sin(kd(n_o - n_e))\cos 2\phi \sin 2\theta + \frac{\epsilon}{2\omega}E_0^2\{1 - \cos(kd(n_o - n_e))\}\sin 2\phi \quad (3)$$

In general, the first term of equation (3) is the torque due to the plane-polarized component of elliptically polarized light while the second term is due to the change in polarization caused by passage through the medium. For plane-polarized light, $\phi = 0$ or $\pi/2$, so the torque on the particle is proportional to $\sin 2\theta$, so that a particle will experience torque so long as θ is non-zero, and will be at equilibrium when the fast axis of the crystal is aligned with the plane of polarization ($\theta = 0$). We found that calcite fragments trapped in plane-polarized light are aligned in a particular orientation, and a particular particle is always aligned in the same plane each time it is trapped. When the plane of polarization is rotated using a half-wave plate, a particle's alignment exactly follows the rotation of the plane of polarization. In Fig. 1, a calcite fragment is shown to rotate through 80° as a half-wave plate controlling the polarization of the trapping beam is rotated through 40°, illustrating the alignment of birefringent particles to the plane of polarization. To our knowledge, this is the first report of an optically trapped particle being rotated through a preset angle; a modification to the set-up whereby the half-wave plate could be spun at a set rate would also allow the particle to rotate at a preset frequency.

The second term of equation (3) will be constant for a given laser power and ellipticity of polarization (characterized by ϕ), and will be maximum for circularly polarized light when the first term vanishes. Hence, when trapped in a circularly polarized beam, a birefringent particle will experience constant torque. In a viscous medium, this torque will be balanced by the drag torque, $\tau_D = D\Omega$, where D is the drag coefficient and Ω is the angular speed, so in this case a birefringent particle will rotate with constant frequency and angular speed. We measured the rotation frequencies of trapped

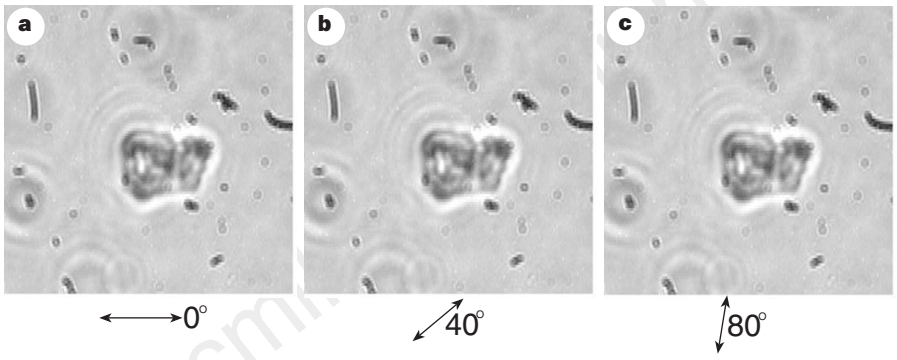

Figure 1 Three sequential photographs (frames) of a trapped calcite crystal, showing alignment with the plane of polarization of the trapping beam. A λ/2 plate was rotated by 20° between successive photographs, rotating the plane of polarization by 40°, as shown by the arrows, and exerting an alignment torque on the crystal, causing it to rotate to a new position. This can be used to rotate the particle at a controlled speed, or to control its orientation.

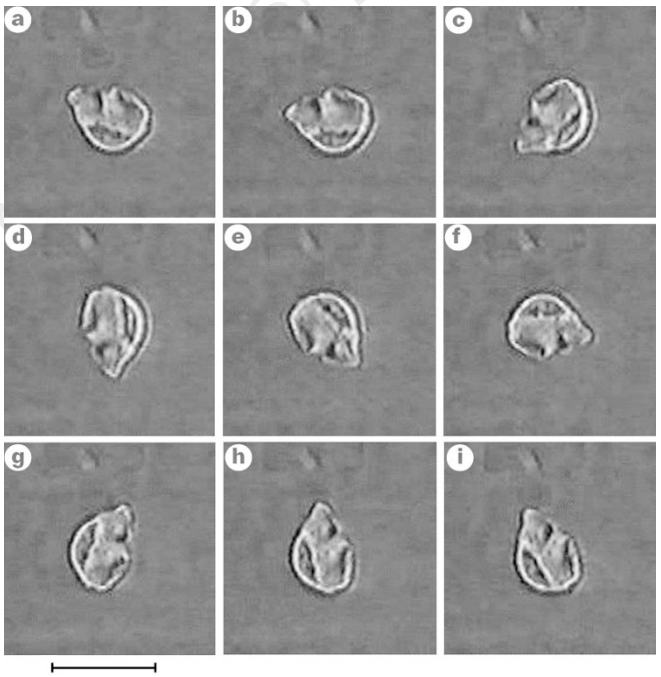

Figure 2 Nine frames of a trapped calcite crystal, showing free rotation due to an elliptically polarized trapping beam. The speed of rotation is limited by the viscous drag on the particle. As the optical torque acting on the particle depends on its orientation, the rotation speed is not constant. The frames are 40 ms apart. Scale bar, 10 μm.

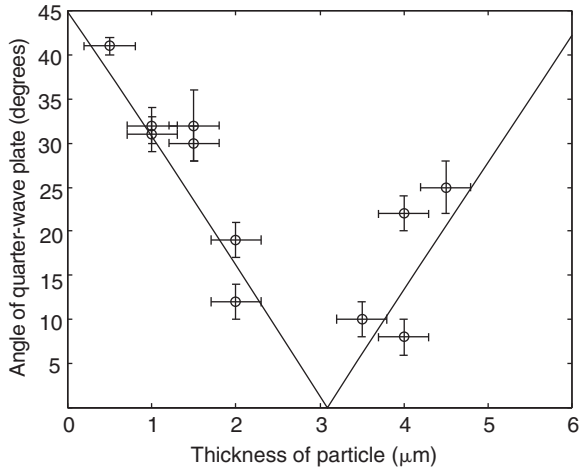

Figure 3 The degree of circular polarization required to cause spinning of a trapped particle depends on its thickness. Here we compare measurements of the minimum angle required for rotation with the theoretical solution. Only if the particle is the exact thickness of a half-wave plate will it always spin in elliptical light. For all other particle thicknesses, there is some angle θ for which the maximum alignment torque will be greater than the spinning torque. The degree of ellipticity of polarization (measured by ϕ) required for the onset of rotation is found from the case where the alignment torque is maximum and the total torque is zero, which is when $\sin[kd(n_o - n_e)]\cos 2\phi = \{1 - \cos[kd(n_o - n_e)]\}\sin 2\phi$. The solution to this is $\phi_{rotate} = [\pi - kd(n_o - n_e)]/4$. In general a particle will be aligned to the plane of polarization of the trapping beam unless there is sufficient torque due to the circularly polarized component to set it into rotation, when it will experience a position-dependent torque.

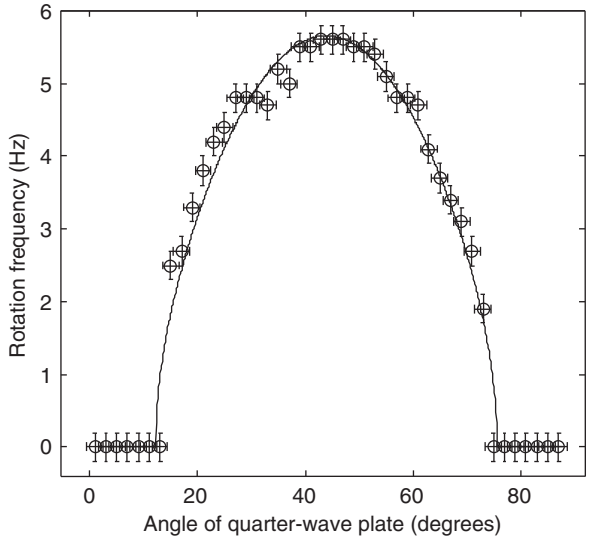

Figure 4 The variation of rotation frequency with the polarization of the trapping beam. The sudden onset of rotation when the minimum angle is reached can be clearly seen. The theoretical response of the particle allows a particle of unknown size to be measured, or can be used to determine the viscosity of a fluid. In this case, the trapping beam has a power of 50 mW, and the particle is 6.15 μm in radius and 2.3 μm thick. The frequency of rotation for a trapping beam of power P and optical frequency ω is $f = [\mathrm{Re}(P\{[1 - \cos kd(n_o - n_e)]^2 \sin^2 2\phi - \sin^2 kd(n_o - n_e)\cos^2 2\phi\}^{1/2})]/(2\pi\omega D)$. The drag torque coefficient D can be estimated by representing the particle as an ellipsoid[6]. The drag will lie between that of a sphere of radius a in a medium of viscosity μ ($D = 8\pi\mu a^3$) and a disk of the same radius ($D = (32/3)\mu a^3$). Under the very low Reynolds number flow conditions encountered here, the surface texture and fine structure of the particle are unimportant. The maximum rotation speed, $f = P/\pi\omega D$, will result when the incident light is circularly polarized and the particle is a half-wave plate. Small particles will generally rotate faster due to less drag, but as particles become too small, their thickness becomes much less than the ideal half-wave case, and they will not intercept all of the power available to spin larger particles.

calcite fragments by detection of back-scattered light[1]; the results show that calcite fragments rotate at constant frequency in circularly polarized light, and that this frequency is proportional to the laser power. A rotating particle is shown in Fig. 2. The fastest rotation frequency measured was 357 Hz, for a particle 1 μm thick trapped in a 300-mW laser beam.

For the general case of elliptically polarized light, both the alignment torque and the spinning torque will act, and the effect on the birefringent particle will depend on the thickness d and the ellipticity ϕ of the light. The particle will only rotate if the maximum alignment torque is less than the spinning torque. This is shown in Fig. 3. In Fig. 4 we plot the variation of rotation rate of a larger calcite crystal with degree of ellipticity of the trapping beam ϕ, showing the characteristic behaviour of a birefringent particle in elliptically polarized light.

The agreement between our results and the theory outlined above shows that the calcite particles act as microscopic wave-plates. The measurement of the rotation speed of spinning particles is a less accurate but simpler analogue of Beth's experiment[4]. In particular, assuming conventional viscous drag, the observed speeds are consistent with the accepted intrinsic spin angular momentum of $\hbar$ per photon (see Fig. 4). Our results also show how optical torques can be exerted on certain microscopic objects with high precision and efficiency, with minimal heating. Depending on the details of the arrangement, a constant torque independent of orientation can be exerted, leading to rotation rates up to hundreds of hertz, or alternatively the orientation of the object can be smoothly controlled.

The controllability of the motion of calcite particles and the minimal absorption involved suggests calcite as an ideal material for optically driven rotary micromachines. Such micromachines could include pumps, stirrers, or optically powered cogwheels. The rotation could also be used to study the viscosity of small samples of fluids, or the alignment of calcite particles could be used to hold probe particles in particular orientations, which could be useful for atomic-force or other forms of microscopy. The birefringence of biological samples is usually much less than that of calcite, but may sometimes be large enough to allow the same alignment and free rotation to be achieved. □

Received 12 December 1997; accepted 7 May 1998.

1. Friese, M. E. J., Enger, J., Rubinsztein-Dunlop, H. & Heckenberg, N. R. Optical angular-momentum transfer to trapped absorbing particles. *Phys. Rev. A* **54,** 1593–1596 (1996).
2. He, H., Friese, M. E. J., Heckenberg, N. R. & Rubinsztein-Dunlop, H. Direct observation of transfer of angular momentum to absorptive particles from a laser beam with a phase singularity. *Phys. Rev. Lett.* **75,** 826–829 (1995).
3. Simpson, N. B., Dholakia, K., Allen, L. & Padgett, M. J. Mechanical equivalence of the spin and orbital angular momentum of light: an optical spanner. *Opt. Lett.* **22,** 52–54 (1997).
4. Beth, R. A. Mechanical detection and measurement of the angular momentum of light. *Phys. Rev.* **50,** 115–125 (1936).
5. Ashkin, A., Dziedzic, J. M., Bjorkholm, J. E. & Chu, S. Observation of a single-beam gradient force optical trap for dielectric particles. *Opt. Lett.* **11,** 288–290 (1986).
6. Constantinescu, V. N. *Laminar Viscous Flow* (Springer, New York, 1995).

Acknowledgements. This work was supported by the Australian Research Council.

Correspondence and requests for materials should be addressed to T.A.N. (e-mail: timo@physics.uq.edu.au).

High-throughput screening of solid-state catalyst libraries

Selim M. Senkan

Department of Chemical Engineering, University of California, Los Angeles, California 90095-1592, USA

Combinatorial synthesis methods allow the rapid preparation and processing of large libraries of solid-state materials. The use of these methods, together with the appropriate screening techniques, has recently led to the discovery of materials with promising superconducting[1], magnetoresistive[2], luminescent[3–5] and dielectric[6] properties. Solid-state catalysts, which play an increasingly important role in the chemical and oil industries[7], represent another class of material amenable to combinatorial synthesis. Yet typically, catalyst discovery still involves inefficient trial-and-error processes[8–10], because catalytic activity is inherently difficult to screen. In contrast to superconductivity, magnetoresistivity and dielectric properties, which can be tested by contact probes, or luminescence, which can be observed directly, the assessment of catalytic activity requires the unambiguous detection of a specific product molecule above a small catalyst site on a large library. Screening by *in situ* infrared thermography[11] and microprobe sampling mass spectrometry[12,13] have been suggested, but the first method, while probing activity, provides no information on reaction products, whereas the second is difficult to implement because it requires the transport of minute gas samples from each library site to the detection system. Here I describe the use of laser-induced resonance-enhanced multiphoton ionization for sensitive, selective and high-throughput screening of a library of solid-state catalysts that activate the dehydrogenation of cyclohexane to benzene. I show that benzene, the product molecule, can be selectively photoionized in the vicinity of the catalytic sites, and that the detection of the resultant photoions by an array of microelectrodes provides information on the activity of individual sites. Adaptation of this technique for the screening of other catalytic reactions and larger libraries with smaller site size seems feasible, thus opening up the possibility of exploiting combinatorial